Milankovitch Period Uncertainties and Their Impact on Cyclostratigraphy

David Waltham (d.waltham@rhul.ac.uk)

Department of Earth Sciences

Royal Holloway

University of London

Egham, Surrey TW20 0EX, UK

Abstract

Astronomically calibrated cyclostratigraphy relies on correct matching of observed sedimentary cycles to predicted astronomical drivers such as eccentricity, obliquity and climate-precession. However the periods of these astronomical cycles, in the past, are not perfectly known because: (i) they drift through time; (ii) they overlap; (iii) they are affected by the poorly constrained recession history of the Moon. This paper estimates the resulting uncertainties in ancient Milankovitch cycle periods and shows that they lead to: (i) problems with using Milankovitch cycles for accurate measurement of durations (potential errors are around 25% by the start of the Phanerozoic); (ii) problems with correctly identifying the Milankovitch cycles responsible for observed period ratios (e.g. the ratio for long-eccentricity/short-eccentricity overlaps, within error, with the ratio for short-eccentricity/precession); (iii) problems with verifying that observed cycles are Milankovitch driven at all (the probability of a random period-ratio matching a predicted Milankovitch-ratio, within error, is 20-70% in the Phanerozoic). Milankovitch-derived ages and durations should therefore be treated with caution unless supported by additional information such as radiometric constraints.

INTRODUCTION

Astronomically calibrated cyclostratigraphy (Hinnov, 2000; Weedon, 2003) has been used to refine the geological time-scale (e.g. Weedon et al., 1999; Gradstein et al., 2004; Peterson, 2011), estimate sedimentation rates (e.g. Meyers, 2008) and improve understanding of sedimentary processes in the past (e.g. Herbert, 1992). There are several approaches but

they are generally equivalent to spotting multiple orders of cyclicity in the sedimentary record and matching their wavelength-ratios to the expected period-ratios of astronomical drivers. For example, “bundling” of packages of five cycles into larger repeated sequences may indicate the sedimentary effects of climate precession (with a period ~20ky) superimposed upon eccentricity (with a period ~100 ky) (Sander, 1936; Schwarzacher, 1947; Goldhammer et al., 1987; Gong et al., 2001). More sophisticated analyses utilize spectral techniques to identify the principal wavelengths in the data (Thomson, 1990; Williams; 1991; Paul et al., 2000; Tian et al., 2014) along with rigorous statistical techniques to reject statistically insignificant identifications and to evaluate uncertainty (e.g. Myers 2012; Hinnov, 2013; Zeeden et al., 2015). It is also possible to independently confirm longer cycles using radiometric dating (Hinnov and Hilgen, 2012; Boulila et al., 2014) and this greatly increases confidence in the analyses. Furthermore, “tuning” can considerably enhance results by forcing exact-regularity onto one of the observed cycles to compensate for fluctuations in sedimentation rate (e.g. Weedon et al. 1999; Huang et al., 2010).

However, Milankovitch cycle periods (and hence their ratios) are imperfectly known in the past and this may cause problems for cyclostratigraphy. In particular, any uncertainties in predicted periods give rise to corresponding uncertainties in estimates of observed time-durations and this, in turn, impacts on attempts to use cyclostratigraphy to refine the geological time-scale. Furthermore, sufficiently large uncertainties in period-ratios would make the hypothesis, that observed cycles are Milankovitch driven, difficult to test as any such contention will lack statistical significance (i.e. there is a high probability of hitting a plausible ratio by chance). It also becomes impossible to unambiguously assign cycles if the

uncertainties are large enough to cause overlaps of adjacent ratios. Incorrect assignment of cycles would, in turn, undermine cyclostratigraphically estimated time-durations.

This paper makes first-order estimates of Milankovitch-period uncertainties so that the potential seriousness of these difficulties can be assessed. It does not discuss the considerable problems associated with analysing sediments to extract periodicities. Instead, it confines itself to issues that will arise even if the wavelengths of sedimentary cycles have been measured with zero error. In practice, data-derived wavelengths are far from perfect but such issues have been discussed by many authors (e.g. Hinnov, 2000 and 2013; Meyers 2013; Vaughan et al., 2012, 2014) and will not be discussed further here.

One source of uncertainty in predicted Milankovitch periods is that the cycles are not perfectly periodic but undergo "diffusive drift" as the mutual interactions between the planets chaotically perturb their orbits over tens of millions of years. For example, using Laskar et al.'s (2011) numerical modelling of the last 100 Ma, the "long eccentricity" variations can be approximated by a sinusoidal signal with a period of 405.6 ky but this period has a drift-generated variation of 2.4 ky. Table 1 shows the principal Milankovitch cycles investigated in this paper, along with their diffusive drift variation (after Laskar et al., 2011). Diffusive drift makes it impossible to extrapolate Earth's detailed orbital parameters more than 40 Ma into the past (Laskar et al. 2004). In particular, the chaotic dynamics of the solar system makes it impossible to predict where we were, in a particular Milankovitch cycle, at distant times. For example, we can say that the ~124 ky eccentricity cycle almost certainly existed at 1 Ga but we cannot say where we were in the cycle, i.e. whether the eccentricity was small or large at that precise time. The current paper therefore estimates

ancient Milankovitch periods but makes no attempt to estimate the amplitudes or phases of ancient Milankovitch cycles.

In addition to diffusive-drift, a further source of uncertainty is that several of the periods shown in Table 1 are sufficiently close to each other to make unique identification difficult. For example, two of the contributing periods to "short eccentricity" lie at 94.9±1.4 ky and 98.9±1.5 ky and so any identified spectral peak in sediments at around 95 ky could be produced by either of these cycles or by a combination of them both.

Uncertainties produced by diffusive drift and by overlap of nearby periods are included in this paper but most of the work reported here concerns another potential source of Milankovitch-period uncertainty; the poorly constrained recession history of our Moon (Webb, 1982; Williams, 1989; Berger et al. 1992; Berger and Loutre, 1994; Sonett et al., 1996; Bills and Ray, 1999; Williams, 2000; Mazumder and Arima; 2005). Friction, from tidally driven ocean currents, gradually slows the Earth's rotation and increases the Earth-Moon separation through time. The falling rotation rate reduces the size of Earth's equatorial bulge whilst lunar-recession produces a drop in tidal-forces and, together, these changes reduce the rate at which Earth's axis precesses. This precession rate is specified by the precession constant, *k*, which gives the change in orientation of the axis in seconds of arc per year ("/y) but which can be converted to a precession period = 1296/*k* thousand years.

Climate-precession cycles and obliquity cycles both result from interaction between axial-precession (which changes the orientation of Earth's axis) and orbital-precession (which changes the orientation of Earth's orbit). Climate precession is produced by the changing relationship between the timing of solstices (as Earth's axis precesses) and the timing of

Earth's closest approach to the Sun (as Earth's orbit precesses). Obliquity cycles, on the other hand, are produced by the changing difference between the orientation of Earth's axis and the orientation of its orbit. Hence, the periods of climate precession and obliquity both change through time as Earth-Moon system evolution produces a changing Earth-axis precession rate. The uncertain recession history of the Moon therefore leads to uncertainty in predicted climate-precession-cycle and obliquity-cycle periods.

To address this problem, ancient obliquity and climate-precession frequencies have previously been estimated by assuming that lunar-recession rate is constant (Berger et al., 1992); Berger and Loutre, 1994) or that the tidal-time-lag (a measure of tidal energy dissipation) is constant (Laskar et al., 2004). Unfortunately, neither assumption is valid. Constant recession at the present-day rate implies Moon formation at ~9.6 Ga whilst assuming that the present-day time-lag applies throughout Earth-history predicts Moon formation at ~1.5 Ga (Gerstenkorn, 1967). In contrast, age estimates for formation of the Earth-Moon system are around 4.5 Ga (e.g. Kleine et al., 2005; Taboul et al., 2007). The modern recession rate therefore overestimates the Earth-Moon separation in the past whilst the modern tidal-time-lag systematically underestimates it.

The underestimated time since Moon-formation, predicted by the constant tidal-time-lag model, implies that correct timing of Moon formation requires the typical tidal-time-lag, over Earth's history, to be substantially smaller than the observed value at the present day. The high, modern tidal-dissipation results from resonance effects in the Earth's oceans; some combinations of natural oscillation frequencies in ocean-basins are close to frequencies excited by the tides (Gotlib and Kagan, 1980, 1981; Platzman et al., 1981; Webb,

1982; Green 2010; Green and Huber, 2013). Hence relatively strong tidal currents are excited which produce increased tidal-friction at the sea-floor.

The strength of this resonance varied through time as a result of eustatic sea-level change, plate-tectonic reorganization of the basins and decreasing tidal-frequency as Earth's rotation slows. Hence, fluctuations in tidal-time-lag (resulting from eustacy and plate-tectonics) are superimposed upon a long-term trend (resulting from a gradually lengthening day). Some studies (e.g. Webb, 1982) imply that the resulting evolution is dominated by the long-term trend whilst others (e.g. Green and Huber, 2013) support the idea of large fluctuations. Settling this question by computer simulation of ancient tides is prevented by the computational-cost of the many, high-resolution models needed and by a lack of sufficiently well-constrained ancient ocean bathymetries. There has been some progress but only for the relatively recent past (e.g. Green and Huber (2013) model Eocene tides) and it is unlikely that sufficiently detailed bathymetries will soon be available for more distant periods of Earth history.

Given these difficulties, it is clearly desirable to find observational constraints on ancient Earth-Moon separation. In principle, these can be obtained using ancient tidal rhythmites; sediments that retain a record of the number of days per neap-spring tide-cycle and the number of neap-spring tide-cycles per year (Williams, 1989, 2000; Sonett et al., 1996a, 1996b; Bills and Ray, 1999; Mazumder and Arima, 2005). The Elatina and Reynella rhythmites of South Australia are the best published examples of tidal rhythmites since they record three independent measurements of Earth-Moon distance (Williams, 1989, 2000; Deubner, 1990). Together, these self-consistent determinations produce a combined separation estimate of 371±2 thousand km at 620±20 Ma.

148 However, as a consequence of errors resulting from missing laminations (Williams, 2000;
149 Archer, 1996) and difficulties with correct recognition of cycles (Archer, 1996; Kvale et al.,
150 1999), other rhythmites are not as well constrained as those from Elatina/Reynella and
151 interpretations of all rhythmite deposits (including Elatina/Reynella) remain highly
152 contentious. Alternate approaches have attempted to use banded iron formations (Walker
153 and Zahnle, 1986) or stromatolites (Vanyo and Awramik, 1985; Cao, 1991) but none of these
154 methods are widely accepted. Thus, there are no uncontentious measurements of Earth-
155 Moon separation except for the present day value.

156 However, one other constraint is available. It is widely, but not universally, accepted that
157 the Earth-Moon system formed as a consequence of a massive impact in the early solar
158 system. This produced debris, orbiting the newly formed Earth, which coalesced to create
159 the Moon just outside the Roche limit (Canup and Asphaug, 2001). Hence, an Earth-Moon
160 separation of around 30 thousand km at 4.5 Ga is reasonably secure. In this paper, these
161 two endpoints (i.e. 384 thousand km today and around 30 thousand km at 4.5 Ga) will be
162 used to constrain reconstructions of Earth-Moon separation though time.

163 This leaves a great deal of uncertainty at other times and the effects of this, on Milankovitch
164 cycle predictions, are the main focus of this paper. This paper does not provide significant,
165 new advances in our understanding of the celestial mechanics of the Earth-Moon system.
166 Neither does it provide new observational constraints. The paper's ambition is simply to
167 take what we already know, and use this to make first-order estimates of uncertainties in
168 cyclostratigraphic frequencies. The paper then looks at the consequences of those
169 uncertainties for cyclostratigraphic interpretation of sediments. It must be emphasised that
170 the uncertainties discussed here result from our ignorance concerning the details of Earth-

Moon system evolution and these uncertainties can in principle be removed by an improved understanding of that history (e.g. through better modelling of ancient tidal-drag or by obtaining better constraints from analysis of ancient sediments). However, such improvements lie outside the scope of this paper which is only concerned with quantifying the level and impact of current uncertainties.

In the next section a range of plausible Earth-Moon separation histories, consistent with the known end-points and celestial mechanics, will be investigated and used to place lower-limits on lunar recession uncertainties through time. Following this, these modelled lunar histories are used to calculate uncertainties in the Earth's axial precession rate. These uncertainties are then combined with those resulting from diffusive-drift and from overlapping-adjacent-periods, to produce estimates of uncertainties in Milankovitch periods and in their ratios. The paper concludes by discussing the resulting impacts on cyclostratigraphy and, in particular, on: (i) estimates of time-durations; (ii) identification of cycles; (iii) testing of the hypothesis that cycles are Milankovitch driven.

LUNAR RECESSION MODELLING

A Simplified Model

The first step is to investigate the Earth-Moon separation history. The theory of lunar recession was developed by Darwin (1880) and modern treatments can be found in Goldreich (1966), Murray and Dermott (1999), Atobe and Ida (2007) and Laskar et al. (2004). These papers provide detailed and comprehensive solutions to the problem of modelling Earth-Moon evolution but, throughout this paper, the simplifying assumptions of a zero-eccentricity, zero-inclination lunar-orbit will be made. These simplifications are necessary

for the methods used here but the errors introduced are insignificant compared to those produced by lunar-recession uncertainty. If solar tides are also neglected (Deubner (1990) shows the effect is small) the evolution of the Earth-Moon separation becomes (Lambeck, 1980; Murray and Dermott, 1999; Bills and Ray, 1999)

$$da/dt = f\, a^{-5.5}, \qquad (1)$$

where a is Earth-Moon separation, t is time and the tidal drag factor, f, is

$$f = 3\,(k_2/Q)\,(m/M)\,R^5\,\mu^{0.5}, \qquad (2)$$

with k_2 the Earth's Love-number (a measure of rigidity), Q the tidal quality factor (a measure of the rate of energy dissipation into heat), m and M the masses of the Moon and Earth respectively, R the radius of the Earth and $\mu = G(M + m)$. (Note that equations (1) and (2) can also be derived from the coplanar, zero-eccentricity, zero-solar-drag approximation to Laskar et al. (2004), equation (12) with Q^{-1} playing a role equivalent to their tidal-lag, Δt.) The stripped-down model given by equation (1) is used in preference to a numerical treatment of the full system of equations because it has the analytical solution

$$a^{6.5} = a_o^{6.5} - 6.5\, F_t\, t \qquad (3)$$

where a_o is the present day lunar distance, t is now age (i.e. there has been a change of sign from t representing time in equation (1)) and F_t is the age-averaged drag factor

$$F_t = \int_0^t f\, dt' / t\,. \qquad (4)$$

This simplified approach is surprisingly accurate as can be seen in Figure 1 which compares its predictions to Laskar et al.'s (2004) full solution. In Figure1, I have assumed a constant tidal drag of $F_t = 2.075 \times 10^{38}$ m$^{6.5}$ s^{-1} (equivalent to Laskar et al.'s (2004) assumption of a constant time-lag of 639 s) which produces an rms difference between the models of only 0.015%.

Model Constraints

The tidal drag factor used in Figure 1 can be validated using lunar laser-ranging (Dickey et al., 1994) which gives a current recession rate of 38.2±0.7 mm/y and hence, from equation (1), $f = 1.99\pm0.04\text{x}10^{38}$ $\text{m}^{6.5}$ s^{-1}. This compares reasonably well to estimates from analysis of eclipse locations from 700 BC to 1990 AD (Stephenson and Morrison, 1995) which give a tidally generated reduction in day-length of 2.3±0.1 ms/century and, by conservation of angular momentum, a lunar-recession rate of 42.1±1.8 mm/y to yield f=2.2±0.1 $\text{x}10^{38}$ $\text{m}^{6.5}\text{s}^{-1}$. Formal combination of these two estimates yields $f = 2.01\pm0.04\text{x}10^{38}$ $\text{m}^{6.5}$ s^{-1} but the larger uncertainty in the eclipse-based estimate may reflect true, longer-term fluctuations not captured by the 40-year lunar-ranging datatset. The remainder of this paper will therefore be conservative by using a slightly larger estimate of uncertainty and assuming a present-day tidal-dissipation of $f = 2.1\pm0.1\text{x}10^{38}$ $\text{m}^{6.5}\text{s}^{-1}$ which encompasses the best estimates from these two approaches and also ensures good agreement with the full model of Laskar et al. (2004). However, in the remainder of this paper, I assume that tidal dissipation varies through time so that F_t is no longer constant. Hence, $F_0 = 2.1\pm0.1\text{x}10^{38}$ $\text{m}^{6.5}\text{s}^{-1}$ but, for all other times, F_t must be estimated.

The first stage is to find F_{4500}, i.e. the drag averaged over the entire history of the Earth-Moon system. Assuming the Moon formed as the result of a large impact at 4500±50 Ma (Touboul et al., 2007) just outside the Roche limit (i.e. a=3±1x10^7 m, Canup and Asphaug (2001)), equation (3) yields $F_{4500} = 6.85\pm0.08\text{ x}10^{37}$ $\text{m}^{6.5}\text{s}^{-1}$ = (0.33±0.03)F_0. The mean tidal drag, averaged over the last 4.5 Gy, is therefore only one third of its present value.

This section will now model a range of plausible lunar-recession histories using equation (3) and the constraints that a_o=3.84x10^8m, F_o=2.1±0.1x10^{38} $\text{m}^{6.5}\text{s}^{-1}$ and $F_{4500} = 6.85\pm0.08\text{ x}10^{37}$ $\text{m}^{6.5}\text{s}^{-1}$. These constraints, along with equation (3), ensure that a middle-path is taken for

the predicted Earth-Moon separation which is neither biased towards too large a value (e.g. as produced by assuming the modern recession rate) nor too small a value (e.g. as produced by assuming a constant tidal-lag-time). Nevertheless, the constraints are not particularly restrictive and allow a wide range of possible scenarios.

To allow progress, this paper investigates two specific scenarios which are compatible with the constraints. First, I assume F_t increases smoothly through time as a consequence of a decelerating Earth-rotation rate. This produces a range of outcomes since the precise form of the smooth function is unknown. Following this, I look at a model in which f is assumed to slowly fluctuate around a long-term mean. This too produces a range of outcomes since there are many fluctuating sequences of f that have a long-term mean equal to F_{4500}.

Between them, these models predict a range of lunar-recession histories. If additional plausible models were also investigated, they could only serve to increase the range of predicted recession histories and so, provided the two models investigated here are plausible, they give a lower-bound estimate on the uncertainty. As will be shown, even this lower-bound is sufficient to demonstrate that astronomically-calibrated cyclostratigraphy is severely compromised.

Smooth Change Model

Ocean-tide models (Gotlib and Kagan, 1980, 1981; Platzman et al., 1981; Webb, 1982) based upon simplified ocean basin geometries (e.g. a constant-depth, hemispherical ocean in Webb (1982)) predict that tidal-drag increases, as Earth's rotation slows, until a resonance peak is reached at a slightly lower tidal-frequency than that experienced today. Thus, in

these simplified models, f has increased through time and has not yet reached its maximum value. The broad effect of this form of f-history on predicted lunar distance can be demonstrated by using exponential growth to approximate this behaviour, i.e.

$$f = f_\infty + (f_0 - f_\infty)\exp(-t/\tau), \qquad (5)$$

where f_∞ is a background value and τ characterizes the timescale over which significant changes in resonance strength occur. This time-scale is poorly constrained, because of the simplifying assumptions of ocean-tide models, but since it is largely controlled by the time-scale for significant changes in Earth rotation rate, it should be on the order of 100s My or longer. Here, I will assume it falls in the range 100 My to 1 Gy.

Equation (3) requires the time-averaged drag F_t, rather than the instantaneous drag f, but integration of equation (5) gives

$$F_t = f_\infty + (\tau / t)(f_0 - f_\infty)[1 - \exp(-t/\tau)]. \qquad (6)$$

The solid lines in Figure 2 show the resulting range of mean-tidal-drag histories with f_∞ chosen to ensure the correct value of F_{4500}. Figure 3 shows the resulting lunar-recession history. Both graphs only show the past 700 Ma because the Phanerozoic is the period of most interest in cyclostratigraphy whilst extending out to 700 Ma allows Figure 3 to compare models to the Earth-Moon distance derived from the Elatina/Reynella rhythmites.

Fluctuating Model

Time variation in f may have been dominated by eustatic sea-level changes or by plate-tectonic reorganization of ocean basins rather than by increasing day-length. Direct modelling of this is problematic, as already indicated, but the little modelling that has been done indicates that small changes in sea-level and basin geometry can produce dramatic changes in tidal dissipation (e.g. see Green and Huber, 2013). Hence, f may be better modelled as a complex fluctuation around a typical value. On this interpretation, the present-day high tidal-dissipation is a chance outlier.

The requirement for positive f, together with a modern value which exceeds the long-term mean by a factor of three, is inconsistent with the assumption that the fluctuations are normally-distributed around the mean but fully consistent with a log-normally distributed process. This subsection therefore builds a tidal-drag model based upon the assumption that drag fluctuated with a log-normal distribution having the correct long-term mean-drag and having fluctuations large enough to allow the high present-day value.

The mean, M, of a log-normal distribution is (DeGroot and Schervish, 2002)

$$M = \exp(m + \sigma^2/2) \qquad (7)$$

where m is the location parameter and σ the scale parameter of the distribution. Furthermore, the cumulative probability is (DeGroot and Schervish, 2002)

$$P(x<X) = \Phi[\{ \ln(X) - m \} / \sigma], \qquad (8)$$

where Φ is the cumulative distribution function of the normal distribution.

Combining equations (7) and (8), the probability of a randomly chosen value being at least three times the mean value is

$$P(x>3M) = 1.0 - \Phi[\, \ln(3)/\sigma + \sigma/2 \,]. \qquad (9)$$

Equation (9) is plotted in Figure 4 as a function of σ and shows that it is plausible for an outlier to exceed the mean by a factor of three (i.e. it has a probability >5%) but only for a narrow range of scale parameter. Hence, a log-normal-fluctuation explanation for the observed, large, modern *f* is statistically plausible (at 5% significance) and the remainder of this section approximates the Earth's tidal-drag history by a time-series of *f*-values extracted from a log-normal process.

The *f*-values in this time-series should be spaced sufficiently far apart that they are uncorrelated, independent specimens from the distribution. The appropriate time-interval depends upon the speed of the process causing changes in resonance strength. The longest relevant time-scale is that for significant reconfiguration of ocean basins whilst the shortest time-scale is associated with eustatic sealevel fluctuations. This unknown time-scale is the main source of uncertainty for the fluctuating-drag model but, in this paper, I will assume values in the range 0 to 100 My.

Over a period significantly greater than the time-scale, the mean value of *f* should converge onto the long-term mean. However, this simple situation is altered because the present-day value is known, rather than extracted from the distribution. As a result, the observed long-term mean is skewed away from the true mean and towards a higher value according to

$$F_{4500} = (nM + f_0) / (n + 1) \qquad (10)$$

where *n* is the sample size, i.e.

$$n = 4500 / \Delta t \quad (11)$$

and Δt is the time-scale of the process (i.e. the gap between uncorrelated f values). Equation (10) allows the true-mean, M, of the distribution to be estimated from the observed long-term mean, F_{4500}. To completely specify the log-normal distribution a scale factor is also needed and I assume σ=1.48 since this gives the distribution for which the modern high-drag is least unlikely.

Given M and σ, the envelope of reasonable F_t functions can be found by noting that, for normal distributions, the sample mean fluctuates with a standard error equal to standard-deviation/$\sqrt{n}$ (where n is sample size). Thus, for a log-normal distribution, the sample mean fluctuates around the population mean, M, with an asymmetric spread given by $M\exp(\pm\sigma/\sqrt{n})$ (i.e. ~68% of the sample means will lie in the range $M\exp(-\sigma/\sqrt{n})$ to $M\exp(+\sigma/\sqrt{n})$). Adding the constraint that f_0 is known then gives

$$F_{k\Delta t} = [\, f_0 + kM\exp(\pm\sigma/\sqrt{k}) \,] / (\, k + 1 \,) \quad (12)$$

as the envelope of time-averaged drags, F_t, at time $t=k\Delta t$.

The dashed lines in Figure 2 show the resulting envelope of F-histories assuming $0 < \Delta t <$ 100 My. The lower limit corresponds to control by eustatic sea level (fluctuations can occur on time scales << 1 My) whilst the upper limit corresponds to the time-scale for significant reorganization of ocean basins. This fluctuating-drag model produces generally lower predictions for F than the smooth-change model because the values fall towards the long-term mean more quickly as we go back in time. This is expected given that the assumed time-scale for the fluctuating model was 0-100 My whilst the assumed time-scale for the smooth-change model was 100-1000 My.

Comparison of Models and Data

The Earth-Moon separations produced by this paper's models are shown in Figure 3 along with the results from analysis of the tidal-rhythmites at Elatina/Reynella discussed in the introduction. The results of modelling lunar-recession assuming a constant tidal drag factor (i.e. the model of Laskar et al. (2004)) are also shown for comparison. The key observations are that the models introduced in this paper show significantly greater Earth-Moon separation than the constant-drag-factor model and much better agreement with the rhythmite data. Furthermore, the generally smaller drag-values of the fluctuating-drag model, compared to the smooth-change model, results in generally higher Earth-Moon separations at any given moment in time. This is the consequence of the smaller time-scale in the fluctuating model, as discussed above.

EARTH'S AXIAL PRECESSION FREQUENCY

The next step is to calculate Earth's precession frequency from the Earth-Moon separations found above. Following the methods described in Berger et al. (1992) but, as before, assuming a circular lunar-orbit, the axial precession frequency, k, is

$$k = A \cos(o)\, \Omega\, [\, (m/a^3) + (m_{\odot}/a_{\odot}^{\,3}) \,] \qquad (13)$$

where A is a constant (chosen to make present day k=50.476 "/y, after Laskar et al. (2004)), o is obliquity, Ω is Earth's rotation frequency and $\odot$ indicates solar values. Earth's rotation rate and the obliquity can be calculated using the approach of Goldreich (1966) and Atobe and Ida (2007) which, under this paper's standard assumptions of circular, coplanar orbits and small solar effects, simplify to the equations

$$dx/da = -h(1 - x^2)(\Omega x - 2n) / 4aCx\Omega (\Omega x - n) \quad (14)$$

$$Cx\Omega = L_o - h \quad (15)$$

where C is Earth's moment of inertia, x=cos(o), h is the angular momentum of the lunar orbit (=$m'\mu^{1/2}a^{1/2}$), n is the lunar mean motion (=$\mu^{1/2}a^{-3/2}$), L_o is the conserved total angular momentum perpendicular to the lunar orbit, m' is the reduced lunar mass (=$mM/(m+M)$) and μ=G(m+M). Explicit finite-difference solution of these equations (Press et al., 2002) gives Figure 5 which is indistinguishable from the full solution shown graphically in Goldreich (1966).

Using equations (13), (14) and (15), together with the previously derived results for lunar-recession, then produces the Earth-axis precession history shown in Figure 6. The key observation, from the point of view of this paper, is that the uncertainty in k increases with age and reaches around 10 "/yr by the early Phanerozoic.

THE IMPACT ON CYCLOSTRATIGRAPHY

Figure 7 shows the obliquity and climate-precession periods, along with their uncertainties, that result from combining Table 1 with Figure 6. Note that two of the climate-precession cycles given in Table 1 (P3 and P4) are indistinguishable on this plot and, hence, there are only four distinct cycles shown. The main conclusion is that the uncertainty in all the cycles increases rapidly with age, as a consequence of the uncertainty in Earth-Moon separation. Furthermore, by 150 Ma the uncertainties make two of the climate-precession cycles indistinguishable and, by 500 Ma, all of the climate-precession cycles have merged.

For obliquity, uncertainty rises from 0% today to 25% at the beginning of the Phanerozoic (~8 ky from the bottom of the range to the top, centred ~32 ky). As a consequence, any sedimentation durations calculated using obliquity cycles will also have errors of the same relative size and these could undermine attempts to use cyclostratigraphy to refine the geological time-scale.

Similar sized relative-errors also occur for the climate-precession cycles but, in this case, the situation is made more complex by the existence of four separate cycles. Two of the cycles (P3 and P4) are indistinguishable at all times and another two (P1 and P2) become indistinguishable before 150 Ma. All four cycles are indistinguishable before 500 Ma. By the start of the Phanerozic the uncertainty exceeds 35% (~7ky range centred ~19ky).

However, as discussed in the introduction, the true observables determined from analysis of sedimentary cycles are not usually cycle periods but, rather, ratios of sedimentary wavelengths. Figure 8 uses the periods (and associated uncertainties) from Figure 7 to calculate Milankovitch period ratios (and their uncertainties). Note that the 10 cycles listed in Table 1 give rise to 45 ratios but, for clarity, Figure 8 does not display them all. Firstly, related ratios which overlap have been collected together (e.g. the top of Figure 8 shows the 4 long-eccentricity/precession ratios as a single zone). Secondly, the 4 ratios of long-eccentricity/short-eccentricity are not plotted as they do not change with time (after including overlaps, these ratios are 4.19±0.17 and 3.19±0.17).

The first conclusion that can be drawn from Figure 8 is that some period-pairs are non-unique. Before 400 Ma, an observed period ratio of ~4.5 could result from short-eccentricity/precession or short-eccentricity/obliquity. Even more seriously, one of the long-eccentricity/short-eccentricity ratios (4.19±0.17) always overlaps with short-

414 eccentricity/precession whilst the other long-eccentricity/short-eccentricity ratio
415 (3.19±0.17) always overlaps with short-eccentricity/obliquity. As a consequence, there is
416 potential to misidentify cycles. For example, an observed ratio of 4.2 might indicate that
417 the shorter cycle is ~20 ky if it's precession-related or ~100 ky if it's short-eccentricity
418 related. This would produce a five-fold difference in estimated time-duration.

419 A further problem indicated by Figure 8 is that, even at 0 Ma, there is a 20% probability that
420 a randomly chosen ratio will fall within a predicted ratio-range. By the time we get to the
421 start of the Phanerozoic there is a 70% chance of a randomly chosen ratio hitting a
422 predicted Milankovitch-ratio uncertainty range. Under these circumstances, we cannot
423 claim that finding a predicted ratio, in a sedimentary dataset, is a reliable indication that the
424 cycles really are Milankovitch driven. Ideally, for identification of Milankovitch-cyclicity to
425 be statistically significant, the probability of hitting a predicted ratio by chance should be
426 below 5% (taking the standard assumption in Earth Sciences of a 5% significance level).
427 Clearly, from Figure 8, this threshold is never met for a single observed ratio.

428 However, in most analyses of sedimentary data, several superimposed cycles will be
429 observed allowing more than one wavelength-ratio to be estimated. If n independent
430 wavelength ratios are found in the data, the probability of this occurring by chance is p^n
431 where p is the probability of hitting a single ratio by chance. The number of independent
432 ratios is, in turn, given by the number of cycles minus one (e.g. 3 cycles give only 2
433 independent ratios because the third ratio is simply related to the other two). Figure 9
434 shows the number of observed cycles required to bring the joint probability below 5%. For
435 example, at 200 Ma, five different Milankovitch cycles should be identified to make the
436 assumption of Milankovitch cyclicity statistically significant. Given this issue, it is important

437 that additional constraints (e.g. radiometric dates) are available when claims are made of
438 the identification of Milankovitch-driven cycles in sedimentary sequences.

439

440 **CONCLUSIONS**

441 This paper has, for the first time, made estimates of the uncertainties in Milankovitch cycle
442 periods and their ratios. It has also investigated the impacts of these uncertainties on
443 astronomically-calibrated cyclostratigraphy. The key conclusions are:

444 1. Obliquity-cycle and precession-cycle period uncertainties grow with time and are
445 typically 10s of percent within the Phanerozoic. These uncertainties will produce
446 similar sized uncertainties in sedimentation-duration estimates made using
447 cyclostratigraphy.
448 2. These uncertainties in Milankovitch periods are large enough to produce substantial
449 overlaps between adjacent periods. As a consequence, there is frequently ambiguity
450 concerning correct identification of cycles and, hence, serious problems with
451 estimation of sedimentation durations.
452 3. Cyclostratigraphy often relies on identification of ratios of Milankovitch cycle pairs
453 (e.g. 5:1 bundling of eccentricity to precession) rather than direct identification of
454 individual cycles. However, these ratios have substantial uncertainties and the
455 resulting overlaps produce severe non-uniqueness in the identification of cycles.
456 These will translate into substantial uncertainties concerning estimation of
457 durations.

4. Once uncertainties are taken into account, the predicted ratios of Milankovitch cycles cover a large percentage of the available space. Hence, finding a wavelength-ratio in sedimentary cycles which matches predicted Milankovitch-ratios is not statistically significant. Several ratios must therefore be identified before Milankovitch cyclicity can be confidently established and this difficulty gets worse the further back in time we go. Hence, in the absence of independent methods for estimating durations (e.g. radio-active decay based methods), it is difficult to demonstrate that cycles are Milankovitch driven.
5. Previous estimates of lunar recession have systematically overestimated Earth-Moon separation in the past (if they assumed constant recession rate) or systematically underestimated Earth-Moon separation (if they assumed constant tidal time-lag). The estimates produced in this paper do not have either bias and, for the first time, include estimates of uncertainty. They should therefore be used in preference to earlier estimates until better observational constraints become available.
6. The uncertainties for obliquity and climate-precession periods are dominated by the effect of uncertainties in lunar-recession history. Hence, the effectiveness of cyclostratigraphy would be significantly enhanced if better estimates of past Earth-Moon separation could be produced.
7. The calculations used in this paper have been incorporated into a JavaScript program that can be run on any modern browser on any device (Fig 11). The program calculates Earth-Moon separation, day-length, axial precession period, the main obliquity period and the four main climate-precession periods for any time in Earth history. It also gives the corresponding uncertainties. The program is released under a creative commons licence and can be freely downloaded from

http://nm2.rhul.ac.uk/project/cyclostratigraphy-evolution-earth-moon-system/.

Once downloaded, the program can be distributed without restriction.

Acknowledgements: Peter Burgess made invaluable suggestions, concerning the paper's emphasis, after reading an earlier version. The reviewers (Stephen Myers and Linda Hinnov) provided constructive and insightful comments that highlighted several weaknesses and also greatly improved the manuscript's clarity.

References

Archer, A.W., 1996, Reliability of lunar orbital periods extracted from ancient cyclic tidal rhythmites, Earth and Planetary Science Letters, v. 141, p. 1-10.

Atobe, K., and Ida, S., 2007, Obliquity evolution of extrasolar terrestrial planets. Icarus, v. 188, p. 1-17.

Berger, A., Loutre, M.F., and Laskar, J., 1992, Stability of the Astronomical Frequencies Over the Earth's History for Paleoclimate Studies, Science, v. 255, p. 560-566.

Berger, A., and Loutre, M.F., 1994, Astronomical forcing through geological time, *in* de Boer, P.L., and Smith, D.G., eds., Orbital Forcing and Cyclic Sequences, IAS special publication, v. 19, p. 15-24.

Bills, B.G., and Ray, R.D., 1999, Lunar Orbital Evolution: A Synthesis of Recent Results, Geophysical Research Letters, v. 26, p. 3045-3048.

Boulila, S., Galbrun, B., Huret, E., Hinnov, L.A., Rouget, I., Gardin, S., Huang, C., and Bartolini, A., 2014, Astronomical calibration of the Toarcian Stage: implications for sequence stratigraphy and duration of the early Toarcian OAE, Earth and Planetary Science Letters, v. 386, p. 98-111.

Canup, R.M., and Asphaug, E., 2001, Origin of the Moon in a giant impact near the end of the Earth's formation, Nature, v. 412, p. 708-712.

Cao, R., 1991, Origin and order of cyclic growth patterns in matministromatolite bioherms from the Proterozoic Wumishan formation, North China. Precambrian Research, v. 51: p. 167-178.

Darwin, G.H., 1880, On the Secular Changes in the Elements of the Orbit of a Satellite Revolving about a Tidally Distorted Planet, Philosophical Transactions Royal Society London,. v. 171, p.713-891.

513 DeGroot, M.H., and Schervish, M.J., 2002, Probability and Statistics, Addison Wesley,
514 Boston, 816p.
515 Deubner, F-L., 1990, Discussion on Late Precambrian tidal rhythmites in South Australia and
516 the history of the Earth's rotation, Journal Geological Society, v. 147, p. 1083-1084.
517 Dickey, J.O., Bender, P.L., Faller, J.E., Newhall, X.X., Ricklefs, R.L., Ries, J.G., Shellus,
518 P.J., Veillet, C., Whipple, A.L., Wiant, J.R., Williams, J.G., and Yoder C.F., 1994,
519 Lunar laser ranging: A continuing legacy of the Apollo Program, Science, v. 265, p. 482-
520 490.
521 Gerstenkorn, H., 1969, The earliest past of the Earth-Moon system. Icarus, v. 11, p. 189-207.
522 Goldhammer, R.K., Dunn, P.A., and Hardie, L.A., 1987, High-frequency Glacio-Eustatic
523 Sealevel Oscillations with Milankovitch Characteristics Recorded in Midlle Triassic
524 Platform Carbonates in Northern Italy, Americam Journal of Science, v. 287, p. 853-892.
525 Goldreich, P., 1966, History of the Lunar orbit, Reviews of Geophysics, v. 4, p. 411-439.
526 Gong, Y., Li, B., Wang, C., and Wu, Y., 2001, Orbital cyclostratigraphy of the Devonian
527 Frasnian-Famennian transition in South China, Palaeogeography, Palaeoclimatology,
528 Palaeoecology, v. 168, p. 237-248.
529 Gotlib, V.Yu., and Kagan, B.A., 1980, Resonance periods of the World Ocean, Doklady
530 Akademii Nauk SSSR, v. 252, p. 725-728.
531 Gotlib, V.Yu., and Kagan, B.A., 1981, On the resonance excitation of semidiurnal tides in the
532 World Ocean, Izvestia Akadamii Nauk SSSR Fizika Atmosferi I Okeana, v. 17, p. 502-
533 512.
534 Gradstein, F., Ogg, J., and Smith, A., 2004, A geologic time-scale 2004: Cambridge,
535 Cambridge University Press, 589 p.
536 Green, J.A.M., and Huber, M. 2013, Tidal dissipation in the early Eocene and implications
537 for ocean mixing, Geophysical Research Letters, v. 40, doi:10.1002/grl.50510.

538 Herbert, T.D., 1992, Paleomagnetic calibration of Milankovitch cyclicity in Lower
539 Cretaceous sediments, Earth and Planetary Science Letters, v. 112, p. 15-28.
540 Hinnov, L., 2000, New perspectives on orbitally forced stratigraphy, Annual Review Earth
541 Planetary Science, v. 28, p. 419–75.
542 Hinnov, L.A., and Hilgen, F., 2012, Chapter 4: Cyclostratigraphy and Astrochronology, in
543 Gradstein, F., Ogg, J., Ogg, G., Smith, D., eds., A Geologic Time Scale 2012, Elsevier,
544 p. 63-83.
545 Hinnov, L.A., 2013, Cyclostratigraphy and its revolutionizing applications in the Earth and
546 planetary sciences, GSA Bulletin, v. 125, p. 1703-1734, doi: 10.1130/B30934.1.
547 Huang, C., Hesselbo, S.P., and Hinnov, L.A., 2010, Astrochronology of the Late Jurassic
548 Kimmeridge Clay (Dorset, England) and implications for Earth system processes, Earth
549 Planetary Science Letters, v. 289, p. 242-255.
550 Kleine, T., Palme, H., Mezger, K., and Halliday, A.N., 2005, Hf-W Chronometry of Lunar
551 Metals and the Age and Early Differentiation of the Moon, Science, v. 310, p. 1671-
552 1674, DOI: 10.1126/science.1118842.
553 Kvale, E.P., Johnson, H.W., Sonett, C.P., Archer, A.W., and Zawistoki, A., 1999, Calculating
554 lunar retreat rates using tidal rhythmites, Journal of Sedimentary Research, v. 69, p.
555 1154-1168.
556 Lambeck, K., 1980, The Earth's Variable Rotation, CUP, Cambridge.
557 Laskar, J., 1999, The limits of Earth orbital calculations for geological time-scale use,
558 Philosophical Transactions Royal Society London. A, v. 357, p. 1735-1759.
559 Laskar, J., Robutel, P., Joutel, F., Gastineau, M., Correia, A.C.M., and Levrard, B., 2004, A
560 long-term numerical solution for the insolation quantities of the Earth, Astronomy and
561 Astrophysics, v. 428, p. 261-285.

562 Laskar, J., Fienga, A., Gastineau, M., and Manche, H., 2011, La2010: a new orbital solution
563 for the long-term motion of the Earth, Astronomy and Astrophysics, v. 532, DOI:
564 10.1051/0004-6361/201116836.
565 Mazumder, R and Arima, M., 2005, Tidal rhythmites and their implications, Earth Science
566 Reviews, v. 69, 79-95.
567 Meyers, S.R., 2008, Resolving Milankovitch controversies: The Triassic Latemar Limestone
568 and the Eocene Green River Formation, Geology, v. 36, p. 319-322, doi:
569 10.1130/G24423A.1.
570 Meyers, S.R., Sageman, B.B., and Pagani, M., 2008, Resolving Milankovitch: Consideration
571 of signal and noise, American Journal of Science, v. 308, p. 770-786, doi:
572 10.2475/06.2008.02.
573 Meyers, S.R., 2012, Seeing red in cycle stratigraphy: Spectral noise estimation for
574 astrochronology. Paleoceanography, v. 27, doi: 10.1029/2012PA002307.
575 Murray, C.D., and Dermott, S.F., 1999, Solar System Dynamics, Cambridge University
576 Press, New York, 592 p.
577 Paul, H.A., Zachos, J.C., Flower, B.P., and Tripati, A., 2000, Orbitally induced climate and
578 geochemical variability across the Oligocene/Miocene boundary, Palaeoceanography, v.
579 15, p. 471-486.
580 Peterson, J.A., 2011, Better mathematical constraints on ages of Carboniferous stage
581 boundaries using radiometric tuff dates and cyclostratigraphy, Geochemistry,
582 geophysics, geosystems, v. 12, doi:10.1029/2010GC003467.
583 Platzman, G.W., Curtis, G.A., Hansen, K.S., and Slater, R.D., 1981, Normal modes of the
584 World Ocean. Part II. Description of modes in the period range 8 hours to 80 hours,
585 Journal of Physical Oceanography, v. 1, p. 579-603.

586 Press, W.H., Teukolsky, S.A., Vetterling, W.T., and Flannery, B.P. 2002, Numerical Recipes
587 in C++, Cambridge University Press, Cambridge.
588 Sander, B. 1936, Beiträge zur Kenntnis der Anlagerungsgefüge (Rhythmische Kalke und
589 Dolomiten aus Tirol), Tschermaks Mineralogische und Petrographische Mitteilungen,
590 v.46, p. 27-209.
591 Schwarzacher, W., 1947, Ueber die sedimentare Rhythmik des Dachsteinkalkes von Lofer,
592 Geolische Bundesanstalt., Vien, 1947, 10-12, 175-188.
593 Sonett, C.P., Kvale, E.P., Zakharian, A., Chan, M.A., and Demko, T.M., 1996a, Later
594 Proterozoic and Paleozoic Tides, Retreat of the Moon, and Rotation of the Earth,
595 Science, v. 273, p. 100-104.
596 Sonett, C.P., Zakharian, A., and Kvale, E.P., 1996b, Ancient tides and length of day:
597 correction, Science, v. 274, p. 1068-1069.
598 Stephenson, F.R., and Morrison, L.V., 1995, Long-term Fluctuations in the Earth's Rotation:
599 700 BC to AD 1990, Philosophical Transactions Royal Society A, v. 351, p. 165-202.
600 Thomson, D., J. 1990, Quadratic-Inverse Spectrum Estimates: Applications to
601 Palaeoclimatology, Philosophcal Transactions: Physical Sciences and Engineering, v.
602 332(1627), p. 539-597.
603 Tian, S., Chen, Z., and Huang, C., 2014, Orbital Forcing and Sea-Level Changes in the
604 Earliest Triassic of the Meishan Section, South China. Journal Earth Science, v. 25, p.
605 64-73.
606 Touboul, M., Kleine T., Bourdon, B., Palme, H., and Wieler, R., 2007, Late formation and
607 prolonged differentiation of the Moon inferred from W isotopes in lunar metals, Nature,
608 v. 450, p. 1206-1209.
609 Vanyo, J.P., and Awramik, S.M., 1985, Stromatalites and Earth-Sun-Moon Dynamics,
610 Precambrian Research, v. 29, p. 121-142.

611 Vaughan, S., Bailey, R. J., and Smith, D. G., 2011. Detecting cycles in stratigraphic data:
612 Spectral analysis in the presence of red noise, Paleoceanography, v. 26, PA4211,
613 doi:10.1029/2011PA002195.
614 Vaughan, S., Bailey, R. J., and Smith, D. G., 2014. Cyclostratigraphy: data filtering as a
615 source of spurious .spectral peaks. From: Smith, D. G., Bailey, R. J., Burgess, P.M., and
616 Fraser, A. J. (eds) Strata and Time: Probing the Gaps in Our Understanding. Geological
617 Society, London, Special Publications, v. 404, doi:10.1144/SP404.11
618 Walker, J.C.G., and Zahnle, K.J., 1986, Lunar nodal tide and distance to the Moon during the
619 Precambrian, Nature, v. 320, p. 600-602.
620 Webb, D.J., 1982, Tides and the evolution of the Earth-Moon system, Geophysical Journal
621 Royal Astronomical Society, v. 70, p. 261-271.
622 Weedon, G.P., Jenkyns H.C., Coe, A.L., and Hesselbo, S.P., 1999, Astronomical calibration
623 of the Jurasic time-scale from cyclostratigraphy in British mudrock formations,
624 Philosophical Transactions Royal Society London, v. A357, p. 1787-1813.
625 Weedon, G.P., 2003, Time-Series Analysis and Cyclostratigraphy, CUP, Cambridge.
626 Williams, G.E., 1989, Late Precambrian tidal rhythmites in South Australia and the history of
627 the Earth's rotation, Journal Geological Society, v. 146, p. 97-111.
628 Williams, G.E., 1991, Milankovitch-band cyclicity in bedded halite deposits
629 contemporaneous with Late Ordovician-Early Silurian glaciation, Canning Basin,
630 Western Australia, Earth and Planetary Science Letters, v. 103, p. 143-155.
631 Williams, G.E., 2000, Geological constraints in the precambrian history of Earth's rotation
632 and the Moon's orbit, Reviews of Geophysics, v. 38, p. 37-59.
633 Zeeden, C, Myers, S.R., Lourens, L.J., and Hilgen, F.J., 2015, Testing astronomically tuned
634 age models. Paleoceanography, v. 30, doi: 10.1002/2014PA002762.
635

636 **Figure Captions**

637 Figure 1. Comparison of equation (3) to the full numerical solution of Laskar et al. (2004).
638 The rms difference is 0.015%.

639 Figure 2. Time-averaged tidal-drag factor, *F*, through time. Solid lines show the plausible
640 range assuming tidal drag has risen smoothly through time. Dashed lines show the plausible
641 range assuming the drag factor has fluctuated through time.

642 Figure 3. Lunar-recession history. Solid lines and dashed lines correspond to equivalent
643 lines from Figure 2. The single point, with error bars, shows results from analysing the
644 Elatina/Reynella rhythmites. The dotted line shows the constant-drag model (i.e. the model
645 of Laskar et al. (2004)).

646 Figure 4. Probability of the modern tidal-drag exceeding three-times the long-term mean,
647 as a function of log-normal scale parameter, σ. This probability exceeds 5% for a (narrow)
648 range of σ and it is therefore plausible that the modern high value represents an outlier
649 from a log-normal distribution.

650 Figure 5. Obliquity of Earth's axis as a function of Earth-Moon separation. Calculations
651 assumed a circular lunar orbit and neglected solar effects. Separation is expressed in Earth-
652 radii to allow easy comparison to the full solution of Goldreich (1966).

653 Figure 6. Earth's axial precession rate history. Solid lines and dashed lines correspond to
654 those shown in figs. 2 and 3.

655 Figure 7. Climate-precession and obliquity periods, together with uncertainties, as a
656 function of age. Two of the precesion periods (P3 and P4 from Table 1) are combined into a

single range as they are very close to one-another. Note that, by the start of the Phanerozoic, the period uncertainty (i.e. the range) is ~25% of the central estimate for both obliquity and precession.

Figure 8. Ratios of Milankovitch cycles as a function of time. Note that the cycles listed in Table 1 give rise to 45 separate ratios but, since uncertainties produce overlaps in many of these, the ratios are represented by the 5 zones shown here plus two zones for the ratios of long eccentricity to short eccentricity (4.19±0.17 and 3.19±0.17, not shown).

Figure 9. Probability that a randomly chosen ratio will agree, by chance, with a predicted Milankovitch cycle ratio within error. Note that, even at 0 Ma, a single observed ratio is insufficient to give a statistically significant identification (i.e. p>5%).

Figure 10. Number of observed cycles required for a statistically significant attribution to Milankovitch cyclicity. If the number of observed cycles is below this threshold, additional constraints are required (e.g. radiometric dating) to support a claim of Milankovitch cyclicity.

Figure 11. JavaScript Program for calculating ancient Milankovitch periods, and their uncertainties, using the methods described in this paper. The program is available at http://nm2.rhul.ac.uk/project/cyclostratigraphy-evolution-earth-moon-system/ and can be downloaded and redistributed freely.

Table 1. The major Milankovitch cycles, focussed on in this paper, along with their variability resulting from diffusive drift. The present day axial precession rate, k, is taken to be 50.476 "/y. Values in Table 1 are taken from Laskar et al (2011). Letters after precession cycles (P1, P2 etc) refer to abbreviations used in Fig. 7.

Cycle	**Freq ("/y)**	**Present Day Period (ky)**
Long Eccentricity	3.196 ± 0.019	405.6 ± 2.4
Short Eccentricity	13.66 ± 0.20	94.9 ± 1.4
Short Eccentricity	10.46 ± 0.20	123.9 ± 2.6
Short Eccentricity	13.11 ± 0.20	98.9 ± 1.5
Short Eccentricity	9.92 ± 0.20	130.8 ± 2.9
Obliquity	k - 18.848 ± 0.066 ± Δk	40.977 ± 0.086
Climate Precession, P1	k + 4.257482 ± 0.00003 ± Δk	23.678377 ± 0.000013
Climate Precession, P2	k + 7.453 ± 0.019 ± Δk	22.3722 ± 0.0074
Climate Precession, P3	k+ 17.92 ± 0.20 ± Δk	18.950 ± 0.055
Climate Precession, P4	k + 17.37 ± 0.20 ± Δk	19.103 ± 0.056

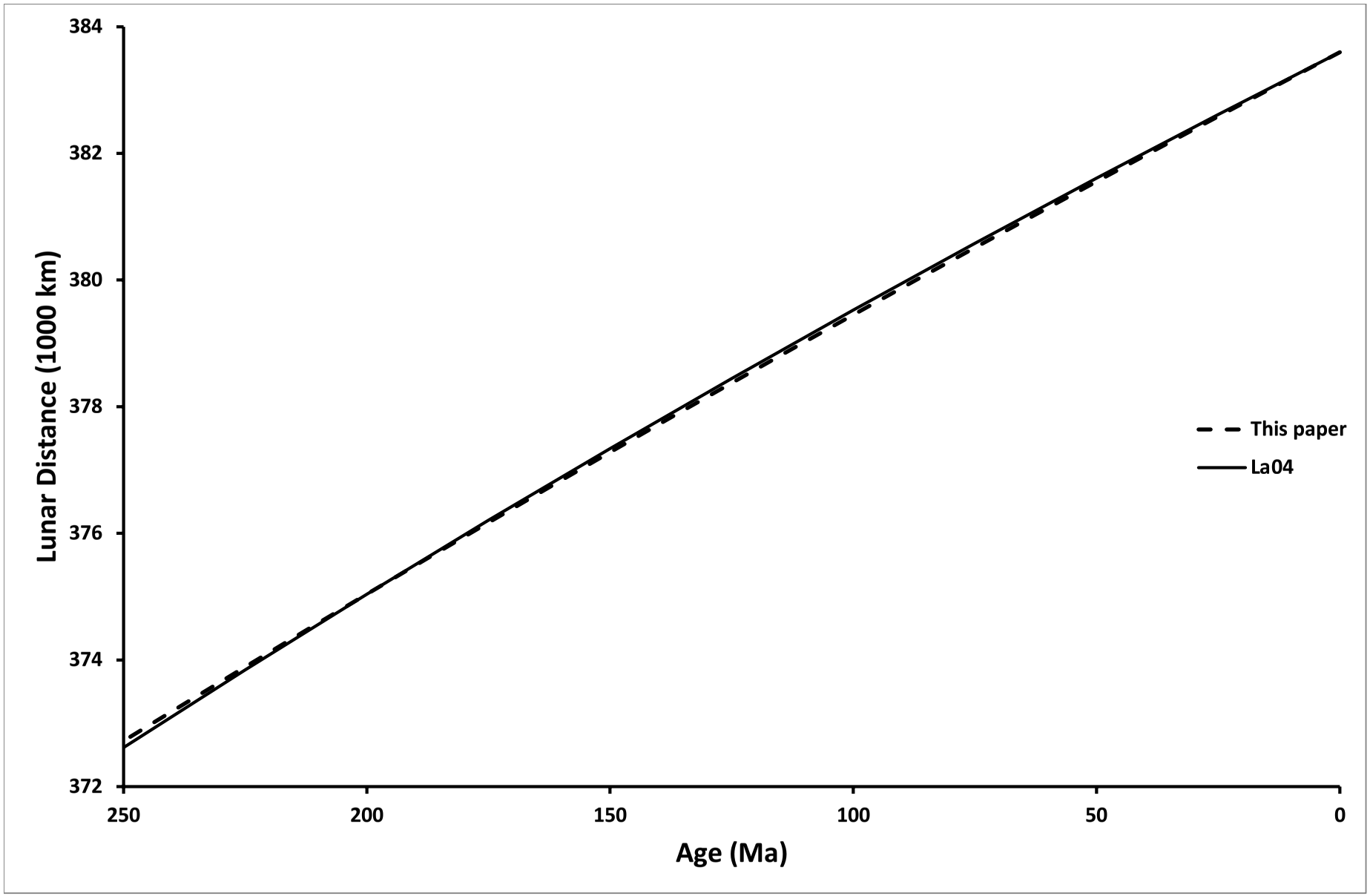
384
382
380
378
376
374
372
Lunar Distance (1000 km)
250
200
150
100
50
0
Age (Ma)
This paper
La04

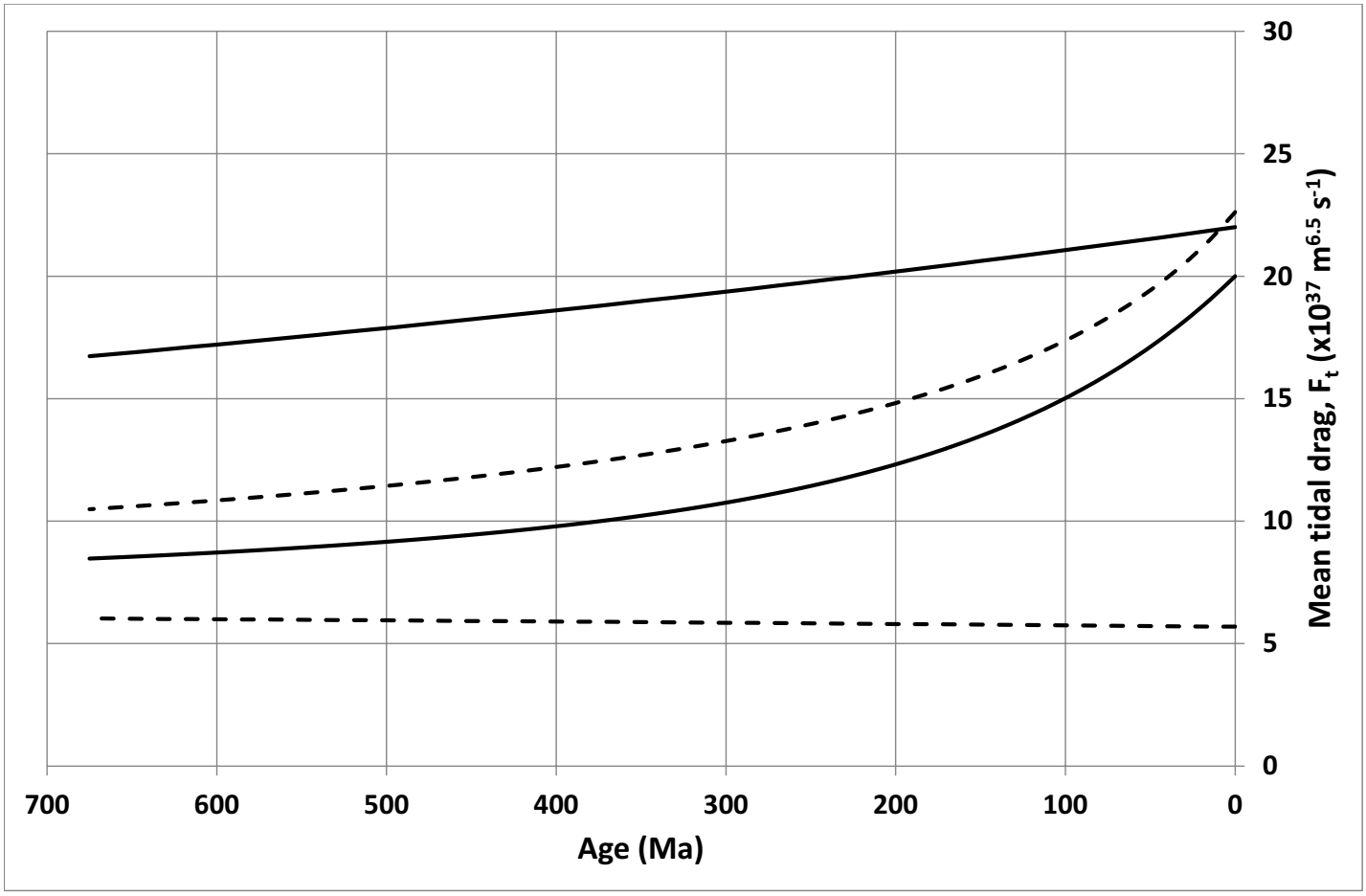
30
25
20
15
10
5
0
Mean tidal drag, F_t (x10^{37} $m^{6.5}$ s^{-1})
700
600
500
400
300
200
100
0
Age (Ma)

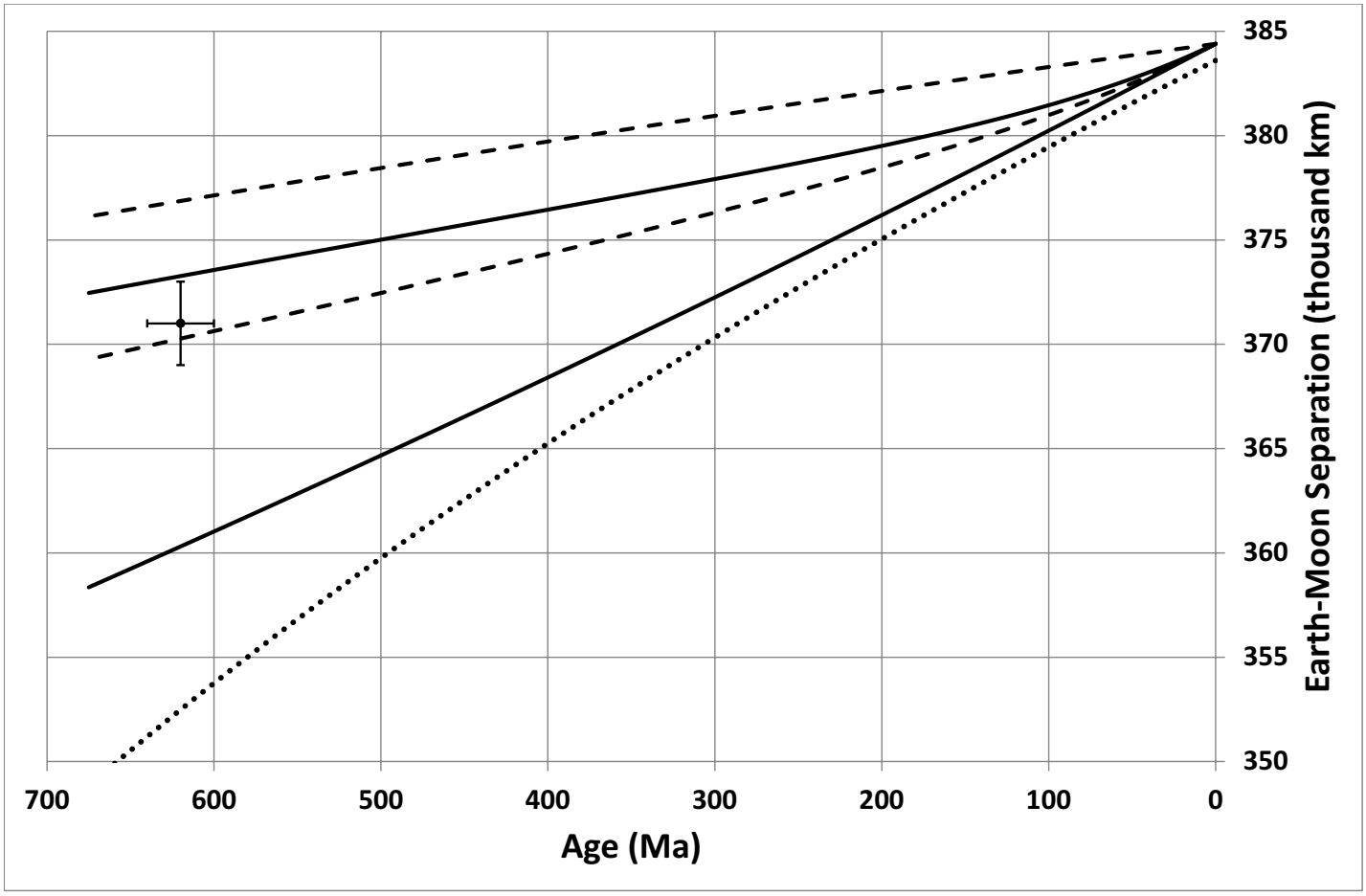
385
380
375
370
365
360
355
350
Earth-Moon Separation (thousand km)
700
600
500
400
300
200
100
0
Age (Ma)


8%
7%
6%
5%
4%
3%
2%
1%
0%
P(x > 3M)
0
0.5
1
1.5
2
2.5
3
3.5
4
σ

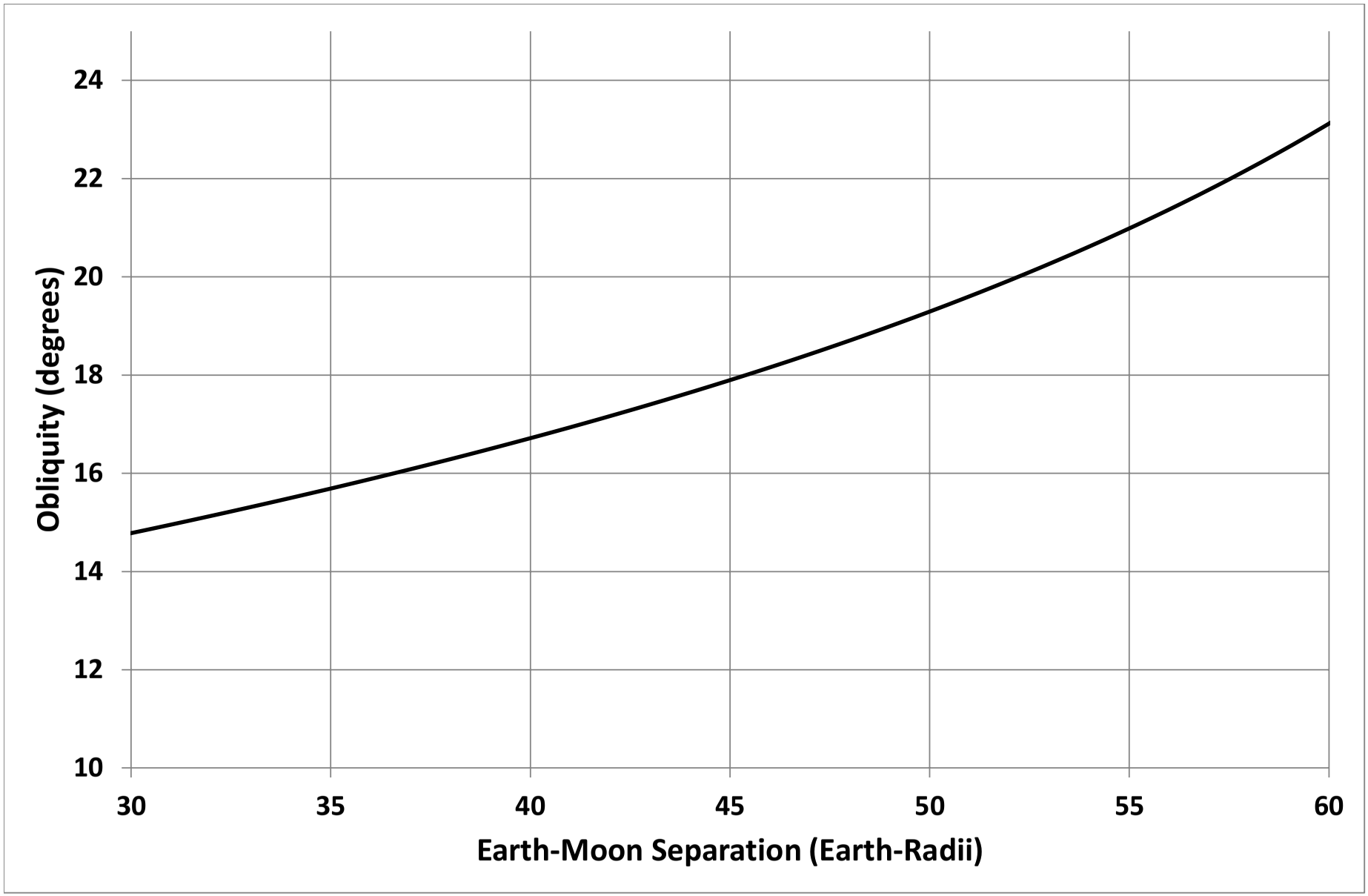
Obliquity (degrees)
24
22
20
18
16
14
12
10
30
35
40
45
50
55
60
Earth-Moon Separation (Earth-Radii)

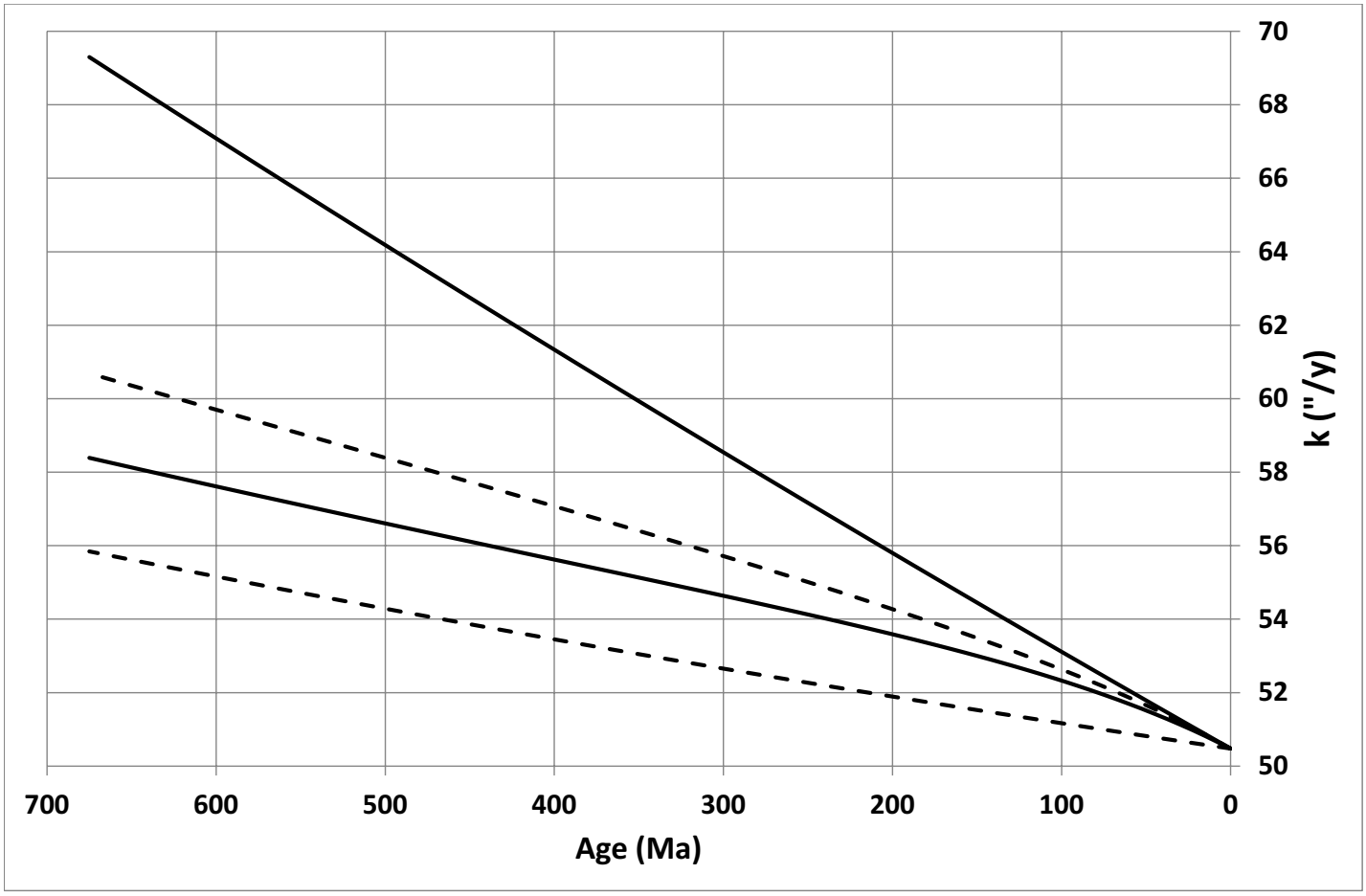
70
68
66
64
62
60
58
56
54
52
50
k (''/y)
700
600
500
400
300
200
100
0
Age (Ma)

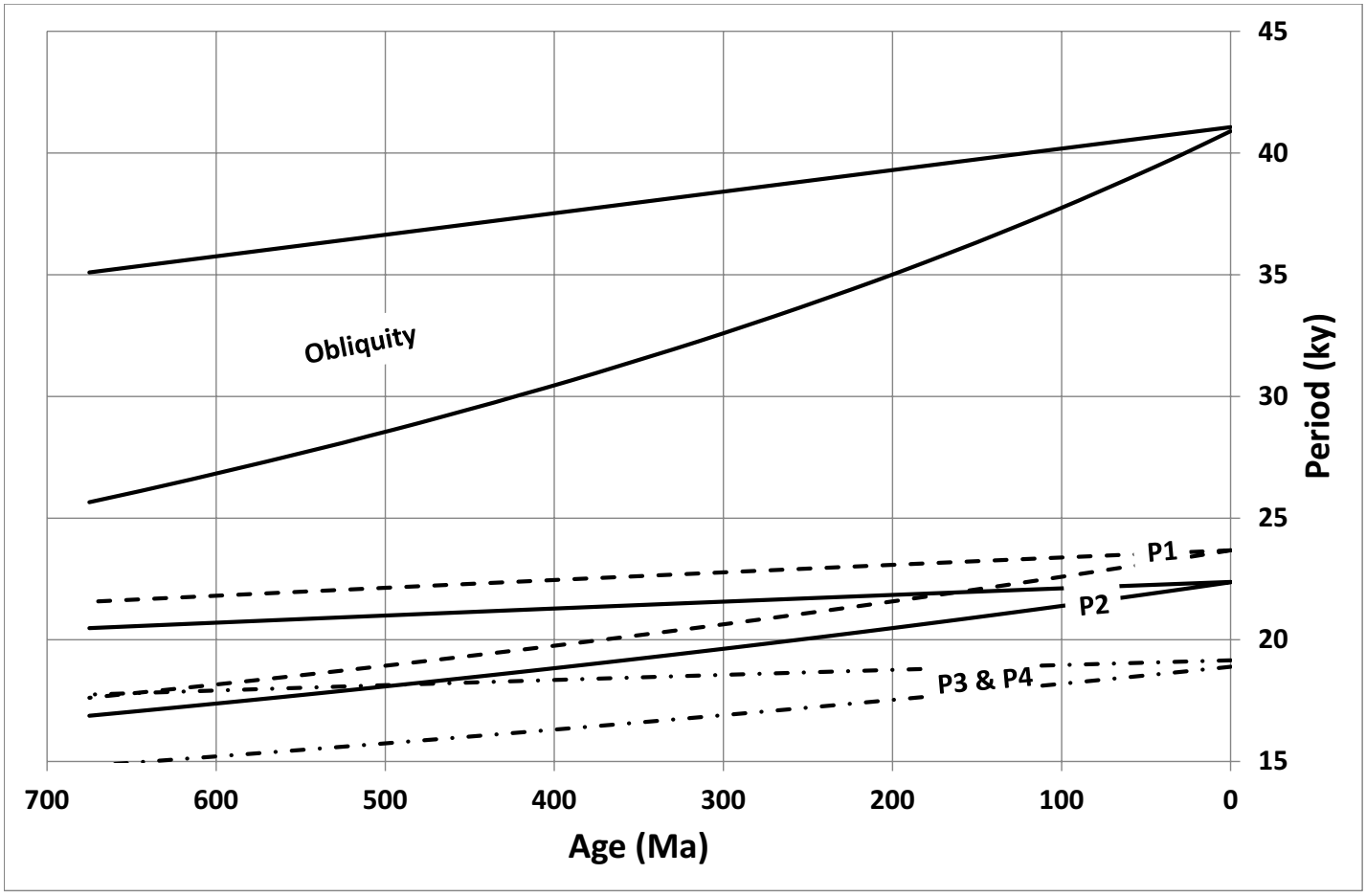
45
40
35
30
25
20
15
Period (ky)
Obliquity
P1
P2
P3 & P4
700
600
500
400
300
200
100
0
Age (Ma)

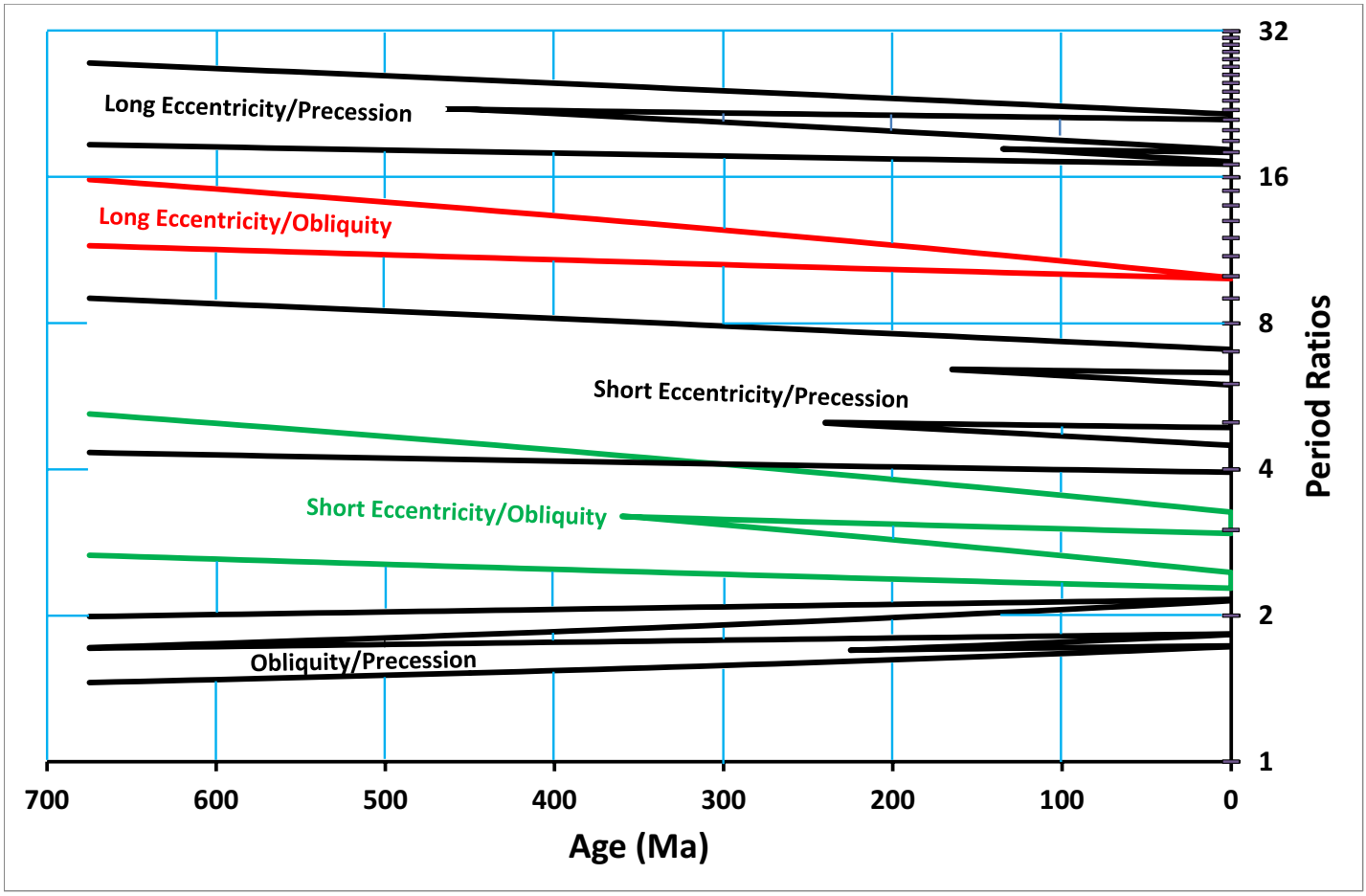
Long Eccentricity/Precession
Long Eccentricity/Obliquity
Short Eccentricity/Precession
Short Eccentricity/Obliquity
Obliquity/Precession
32
16
8
4
2
1
Period Ratios
700
600
500
400
300
200
100
0
Age (Ma)

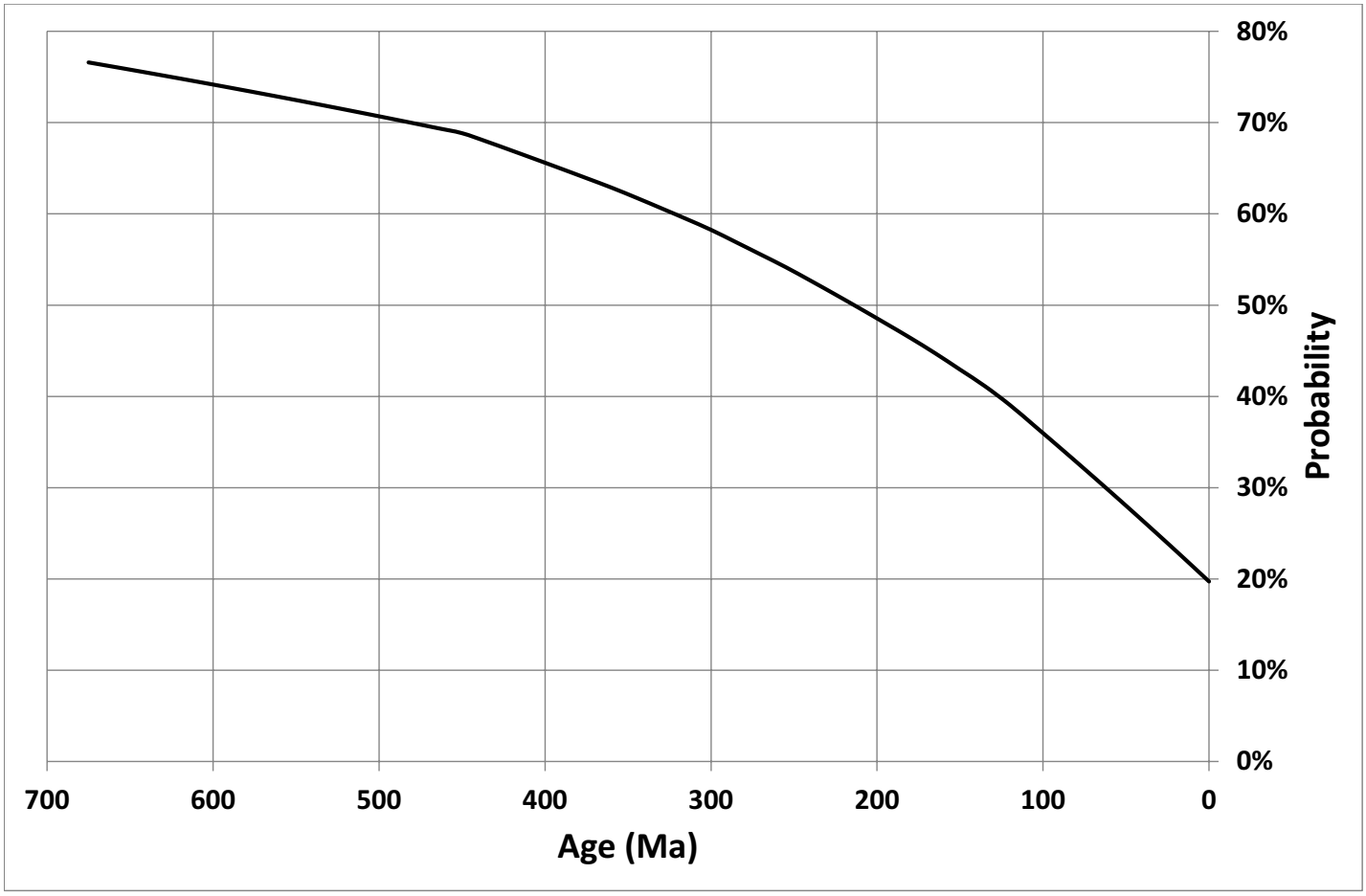
80%
70%
60%
50%
40%
30%
20%
10%
0%
Probability
700
600
500
400
300
200
100
0
Age (Ma)

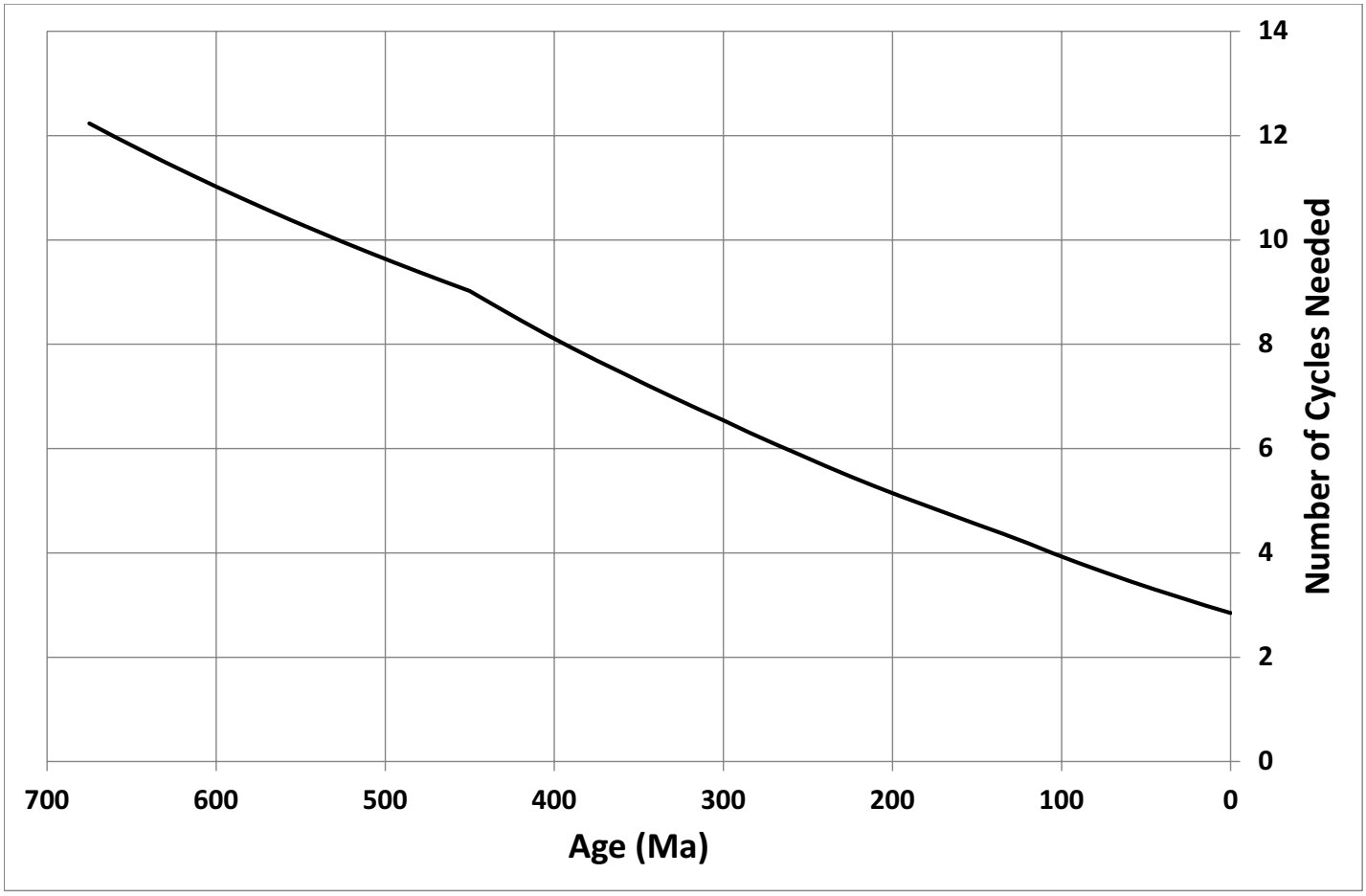
14
12
10
8
6
4
2
0
Number of Cycles Needed
700
600
500
400
300
200
100
0
Age (Ma)

Milankovitch Calculator

Details in:
Waltham, D., 2015. Milankovitch Period Uncertainties and Their Impact on Cyclostratigraphy JSR, in review

Age: 300 Ma

Earth-Moon Distance

376.6 ± 4.4 thousand km

Earth Day

22.88 ± 0.61 hours

Earth Axis Mean Obliquity

22.69 ± 0.31 degrees

Earth Axis Precession Period

23.4 ± 1.2 ky

Main Obliquity Period

35.5 ± 2.9 ky

Climatic Precession Periods

21.7 ± 1.1 ky

20.60 ± 0.97 ky

17.66 ± 0.76 ky

17.88 ± 0.77 ky